Geophys. J. Int. (2002) **148,** 165–178

A test of ray theory and scattering theory based on a laboratory experiment using ultrasonic waves and numerical simulation by finite-difference method

Jesper Spetzler,[1,*] Chadaram Sivaji,[2,†] Osamu Nishizawa[2] and Yo Fukushima[3,‡]

Department of Geophysics, Utrecht University, P.O. Box 80.021, NL-3508 *The Netherlands. E-mail: j.spetzler@citg.tudelft.nl*
Geophysics, Department, Geological Survey of Japan Higashi 1-1-3, *Tsukuba, Ibaraki* 305-8567, *Japan.*
Graduate School of Science, Tohoku University, Aramaki-Aza Aoba, Aoba-ku, Sendai 980-8578, *Japan*

Accepted 2001 June 30. Received 2001 June 6; in original form 2000 November 13

SUMMARY

The structure of the Earth is represented by a wide spectrum of small- and large-scale structures. However, tomographic imaging techniques based on ray theory are often applied inappropriately in models with a characteristic length of heterogeneity smaller than the wavelength and width of the Fresnel zone. In other words, the conditions for ray theory are not satisfied in such models. It is therefore necessary to apply the diffraction theory of waves in tomographic reconstruction techniques in order to retrieve images of the Earth with a more general theory for wave propagation than ray theory. Physically speaking, scattering theory takes the finite-frequency effect of waves into account. We performed a test of ray theory and scattering theory in an ultrasonic wave experiment and in a numerical finite-difference experiment using random media with correlation lengths smaller than the width of the Fresnel zone. We used a stochastic approach to compute the mean squared value of time-shift variations calculated from ray theory and diffraction theory. The theoretical results were compared with the experimental values obtained in the laboratory experiment using rock samples with different length-scales of heterogeneity and from numerical experiments on wave propagation in quasi-random media. We observed that ray theory systematically overestimates the mean squared value of time-shift variations, while the observed statistical values from the laboratory experiments are well predicted by scattering theory. This means that tomographic imaging techniques based on ray theory suffer from a loss of resolution when the reconstructing models have a characteristic length of heterogeneity smaller than the width of the Fresnel zone.

Key words: finite-difference experiment Fresnel zone, ray theory, Rytov approximation, scattering theory, ultrasonic experiment.

1 INTRODUCTION

In this study, we examine ray theory and scattering theory in a laboratory experiment using ultrasonic waves propagating in granite samples with small-scale heterogeneity. Ray theory is a high-frequency theory which is valid if the characteristic length of inhomogeneity is larger than the wavelength and the width of the Fresnel zone. Accordingly, it is only justified to use ray theory in modelling of sufficiently smooth media. On the other hand, people working with seismology (van der Lee & Nolet 1997; Trampert & Woodhouse 1995; Bijwaard & Sparkman 1998; Curtis *et al.* 1998) or with exploration seismics (Parra & Bangs 1992; Goudswaard *et al.* 1998; Hatchell 2000) focus more and more on small-scale structured media for which the conditions for ray theory are generally not satisfied. For such media with heterogeneity comparable or smaller in size than the width of the Fresnel zone, scattering theory of propagating waves is important (Spetzler & Snieder 2001b).

In the past decade much attention has been paid to scattering theory in the literature. Yomogida & Aki (1987), Yomogida (1992), Woodward (1992), Snieder & Lomax (1996) and Spetzler & Snieder (2001b) use the Rytov approximation on the 2-D acoustic wave equation to introduce the effect of finite-frequency in transmitted waves. Marquering *et al.* (1998), Tong *et al.* (1998), Marquering *et al.* (1999), Dahlen *et al.* (2000)

* Now at: Dept. of Applied Earth Sciences, TU Delft, Mijnbouwstraat 120, NL-2628 RZ Delft, The Netherlands
† Now at: Ministry of Science and Technology, Govt. of India, New Mehrauli Road, New Delhi 110 016, India
‡ Now at: CTBTO Data Centre, International Centre P.O. Box 1200, A-1400 Vienna, Austria

© 2002 RAS

and Hung *et al.* (2000) utilise the cross-correlation function to introduce the frequency-depending time-shift in 3-D body wave tomography. In many of these articles, it is shown that scattering theory in 2- and 3-D media predicts that the maximum sensitivity to slowness perturbations is of geometrical ray path. Moreover a paradoxical result is found for the scattering of waves in 3-D; the sensitivity to slowness fluctuations is zero on the ray path. It is a counter-intuitive result compared to ray theory which predicts non-zero sensitivity to the slowness field on the ray path.

Several authors have worked with laboratory experiments using ultrasonic waves. Lo *et al.* (1988) tested the Rytov and Born approximations in vertical seismic profiling (VSP), cross-borehole and surface reflection tomography by using ultrasonic waves propagating in a water tank with gelatin cylinders as scatterers. They found that diffraction tomography is better than ray tomography at reconstructing the model when the size of scatterers is comparable to the wavelength. Schultz & Toksöz (1994) studied scattering from randomly grooved interfaces. Scattering phenomena have been studied in order to understand the attenuation of seismic waves and the generation of coda waves (Dubendorff & Menke 1986; Vinogradov *et al.* 1989; Matsunami 1991; Schultz & Toksöz 1993, 1994)

In this study, we combine the developments in scattering theory with high-quality ultrasonic waveforms measured in a laboratory experiment using samples of Westerly and Oshima granite. The two granites have slowness perturbation fields that can be described using an exponential auto-covariance function, so we can use a stochastic approach to test ray theory and scattering theory in the real laboratory experiment. We compute the ray theoretical and scattering theoretical mean squared value of time-shift fluctuations for exponential random media which are comparable with those obtained from the observed ultrasonic waveforms. In that way, we show that scattering theory is more accurate than ray theory in predicting the observed mean squared value of time-shifts for Westerly and Oshima granite. In addition, we simulate the real laboratory experiment with a 2-D, numerical finite-difference experiment which supports the results found in the ultrasonic wave experiment.

In Section 2, we show how ray theory and scattering theory can be adapted to deterministic and stochastic models. The laboratory experiment is explained in Section 3, while, in Section 4 we describe how the independent determination of the exponential auto-covariance function for Westerly and Oshima granite was carried out. The 2-D numerical experiment is described in Section 5. In Section 6, we present the results from the ultrasonic wave experiment and the numerical experiment, and finally in Section 7 and 8 the discussion and conclusions are given.

2 THEORY

In this section, the mean squared (MS) value of time-shift fluctuations using ray theory and single-scattering theory is derived. We work with two kinds of stochastic media; the exponential random medium which has the auto-covariance function for the slowness perturbation field given by

$$\langle \delta u(\mathbf{r}')\delta u(\mathbf{r}'')\rangle = (\varepsilon u_0)^2 \exp\left(-\frac{r}{a}\right), \tag{1}$$

and the Gaussian random medium with the auto-covariance function for slowness perturbations given by

$$\langle \delta u(\mathbf{r}')\delta u(\mathbf{r}'')\rangle = (\varepsilon u_0)^2 \exp\left(-\left(\frac{r}{a}\right)^2\right). \tag{2}$$

In the two auto-covariance functions in eqs (1) and (2), the reference slowness is denoted by u_0, the root mean squared (rms) value of the relative slowness perturbation field is ε, the correlation length (or roughly the length-scale of heterogeneity) is written as a and $r=|\mathbf{r}'-\mathbf{r}''|$ is the distance between the two points $\mathbf{r}'$ and $\mathbf{r}''$. See Sato (1998) for a thorough description of random media.

2.1 Ray Theory

We follow the idea of Roth *et al.* (1993) to derive the MS-value of time-shift fluctuations based on first order ray perturbation theory (also related to Fermat's principle). The derivation is valid for time-shifts obtained in experiments with 2- and 3-D wave propagation. According to first order ray perturbation theory (Snieder & Sambridge 1992), the time-shift for deterministic slowness perturbation media $\delta u(\mathbf{r})$ is given by

$$\delta t(L) = \int_0^L \delta u(s)ds, \tag{3}$$

where L is the source-receiver distance. The expectation value is taken of the square of the time-shift in eq. (3), so we get the MS-value of time-shift fluctuations $\langle(\delta t)^2\rangle(L)$ due to ray theory.

$$\begin{aligned}\langle(\delta t)^2\rangle(L) &= \int_0^L \int_0^L \langle \delta u(s')\delta u(s'')\rangle ds'ds'' \\ &= 2\int_0^L (L-r)N(r)dr,\end{aligned} \tag{4}$$

where the auto-covariance function $N(r)=\langle \delta u(s')\delta u(s'')\rangle$ and $r=|s'-s''|$. The step to reduce the double integration to a single integration in eq. (4) is explained in Roth (1997).

For the case where the source-receiver distance is much smaller than the correlation length, (i.e. $L/a \ll 1$), the exponential and Gaussian auto-covariance function in eqs (1) and (2) are set to $(\varepsilon u_0)^2$. Hence, the MS-value of time-shift fluctuations is given by

$$\begin{aligned}\langle(\delta t)^2\rangle(L) &\approx 2(\varepsilon u_0)^2 \int_0^L (L-r)dr \\ &= (\varepsilon u_0 L)^2,\end{aligned} \tag{5}$$

which is the same result as for a homogeneous slowness perturbation field.

Next consider the case that the source-receiver offset is much larger than the correlation length, (i.e. $L/a \gg 1$). For the exponential auto-covariance function in eq. (1), the MS-value of time-shift fluctuations is given by

$$\langle(\delta t)^2\rangle(L) = 2(\varepsilon u_0)^2 aL. \tag{6}$$

For Gaussian random media, the MS-value of time-shift fluctuations is found to be

$$\langle(\delta t)^2\rangle(L) = \sqrt{\pi}(\varepsilon u_0)^2 aL. \tag{7}$$

See Roth *et al.* (1993) or Spetzler & Snieder (2001a) for an explanation of how to derive eqs (6) and (7).

Ray theory is valid when the correlation length of heterogeneity is larger than the wavelength λ and the width L_F of the Fresnel zone. In non-dimensional numbers, the conditions for the regime of ray theory are written as

$$\frac{\lambda}{a} \ll 1, \quad \text{and} \quad \frac{L_F}{a} \ll 1. \tag{8}$$

See Menke & Abbot (1990).

2.2 Scattering Theory

The scattering theoretical time-shift $\delta t(L)$ is written as a volume integration of the deterministic slowness perturbation field $\delta u(\mathbf{r})$ multiplied by the sensitivity kernel $K(\mathbf{r})$ due to non-ray geometrical effects (Spetzler & Snieder 2001b). Hence,

$$\delta t(L) = \int_{\mathbf{V}} \delta u(\mathbf{r}) K(\mathbf{r}) dV, \tag{9}$$

where the integration $\int_{\mathbf{V}} \ldots dV$ is written as $\int_0^L \int_{-\infty}^{\infty} \ldots dxdz$ for wave propagation in two dimensions and as $\int_0^L \int_{-\infty}^{\infty} \int_{-\infty}^{\infty} \ldots dxdydz$ for waves propagating in three dimensions. The MS-value of time-shift fluctuations $\langle(\delta t)^2\rangle(L)$ using scattering theory is obtained by taking the expectation value of the squared time-shift in eq. (9), thus

$$\langle(\delta t)^2\rangle(L) = \int_{\mathbf{V}'} \int_{\mathbf{V}''} \langle \delta u(\mathbf{r}') \delta u(\mathbf{r}'') \rangle K(\mathbf{r}') K(\mathbf{r}'') dV' dV''. \tag{10}$$

The 2-D sensitivity kernel for a point source is given by

$$K(x, z) = \sqrt{u_0 L} \int_{v_0-\Delta v}^{v_0+\Delta v} A(v) \sqrt{v} \frac{\sin\left(\pi v u_0 L \frac{z^2}{x(L-x)} + \frac{\pi}{4}\right)}{\sqrt{x(L-x)}} dv, \tag{11}$$

(see Spetzler & Snieder 2001b). The sensitivity kernel in eq. (11) is integrated in the frequency-range $v_0-\Delta v$ to $v_0+\Delta v$, where the normalised power spectrum $\int_{v_0-\Delta v}^{v_0+\Delta v} A(v) dv = 1$. The central frequency is denoted v_0 and the width of the frequency-band is $2\Delta v$. For a constant power spectrum over the frequency-band (i.e. $A(v) = 1/(2\Delta v)$), the scattering sensitivity kernel in eq. (11) can be evaluated analytically (see Appendix A), hence

$$K(x, z) = \frac{\sqrt{u_0 L}}{2\Delta v \sqrt{x(L-x)}} \left[\frac{1}{b} \sqrt{\frac{v}{2}} (\sin(bv) - \cos(bv)) + \frac{1}{b^{3/2}} \sqrt{\frac{\pi}{4}} \left(C\left(\sqrt{\frac{2bv}{\pi}}\right) - S\left(\sqrt{\frac{2bv}{\pi}}\right) \right) \right]_{v_0-\Delta v}^{v_0+\Delta v}, \tag{12}$$

where $b = \pi u_0 L z^2/(x(L-x))$ and the functions C and S are the Fresnel cosine integral and sine integral, respectively. Abramowitz & Stegun (1970) give a description of the Fresnel cosine and sine integrals. The sensitivity kernel for a point source using scattering theory for 3-D wave propagation is given by

$$K(x, y, z) = u_0 L \int_{v_0-\Delta v}^{v_0+\Delta v} A(v) v \frac{\sin\left(\pi v u_0 L \frac{y^2+z^2}{x(L-x)}\right)}{x(L-x)} dv, \tag{13}$$

(see Spetzler & Snieder 2001b, for an explanation of how to derive the 3-D scattering theoretical sensitivity kernel in eq. 13). Assuming a constant power spectrum, the analytical solution of the sensitivity kernel in eq. (13) is found to be

$$K(x, y, z) = \frac{u_0 L}{2\Delta v x(L-x)} \left[-v \frac{\cos(bv)}{b} + \frac{\sin(bv)}{b^2} \right]_{v_0-\Delta v}^{v_0+\Delta v} \tag{14}$$

where $b = \pi u_0 L(y^2 + z^2)/(x(L-x))$, (see Appendix A). The sensitivity kernel due to the scattering of waves propagating in 2-D and 3-D media is shown in Fig. 1(a) and (b), respectively. We have used eq. (12) to compute the 2-D scattering sensitivity kernel and eq. (14) to evaluate the scattering sensitivity kernel for wave propagation in three dimensions. The sensitivity kernels are calculated for the half source–receiver offset for which

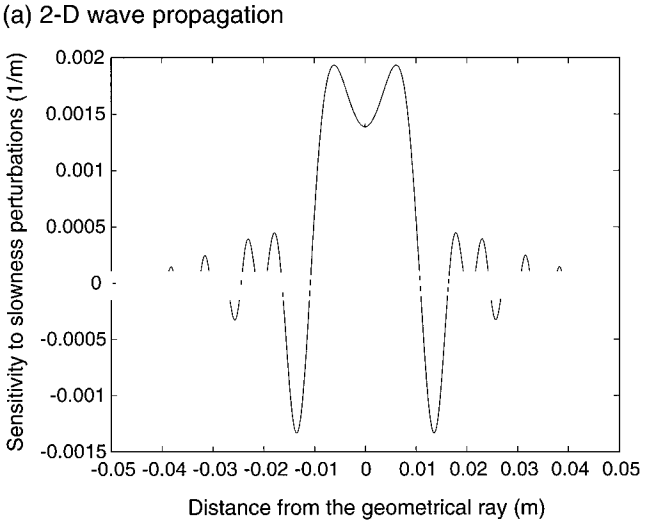

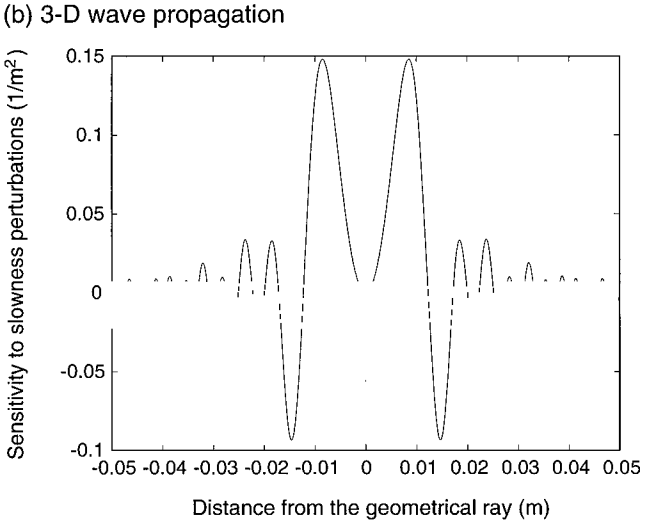

Figure 1. The cross section of the scattering sensitivity kernel. The source–receiver distance $L = 0.08$ m, the reference slowness $u_0 = 2.5 \times 10^{-4}$ sm^{-1}, the central frequency $v_0 = 500$ kHz and the frequency-band $2\Delta v = 400$ kHz. The sensitivity kernels are plotted at the half offset for which the width of the central lobe is maximum. (a) The scattering theoretical sensitivity kernel for a point source due to waves propagating in 2-D. (b) The sensitivity kernel for a point source due to 3-D scattering theory. Notice that scattering theory in 3-D predicts a zero sensitivity to slowness perturbations on the geometrical ray while according to ray theory there is only non-zero sensitivity to slowness perturbations on the ray path.

the central lobe has the maximum width. The source–receiver distance $L = 8$ cm, the central frequency $\nu_0 = 500$ kHz, the half frequency-band $\Delta\nu = 200$ kHz and the reference slowness $u_0 = 2.5 \times 10^{-4}$ sm^{-1}. For both scattering sensitivity kernels in Fig. 1, it is seen that the maximum sensitivity to slowness perturbations is off-path the geometrical ray and that the sensitivity kernels have sidelobes. However, the 2-D scattering kernel is non-zero on the ray path and the 3-D scattering kernel vanishes on the geometrical ray. This is a very counter-intuitive result for wave propagation in three dimensions compared with ray theory which predicts non-zero sensitivity to slowness perturbations on the ray. This result is also found in Tong *et al.* (1998); Marquering *et al.* (1998); Dahlen *et al.* (2000); Hung *et al.* (2000) and Zhao *et al.* (2000) who work with scattering theory in body wave tomography.

Consider the case that the source–receiver distance is smaller than the correlation length, (e.g. $L/a \ll 1$). This limit corresponds to a medium with a homogeneous slowness perturbation so the auto-covariance functions in eqs (1) and (2) can be set to $(\varepsilon u_0)^2$. The MS-value of time-shift fluctuations using 2-D or 3-D scattering theory in eq. (10) is given by

$$\langle(\delta t)^2\rangle(L) = (\varepsilon u_0 L)^2, \tag{15}$$

which is the same result obtained with ray theory in eq. (5). We derive eq. (15) in Appendix B.

Consider instead that the correlation length goes towards zero. It is shown in Appendix C that the MS-value of time-shift fluctuations either using 2- or 3-D scattering theory converges to zero in the limit that the correlation length goes to zero, hence

$$\lim_{a\to 0} \langle(\delta t)^2\rangle(L) \to 0. \tag{16}$$

In this regime, waves propagate in an average medium which is the homogeneous reference medium. The same result can be obtained with eq. (6) for exponential random media and eq. (7) for Gaussian random media using ray theory.

Spetzler & Snieder (2001b) determine in a numerical experiment when the regime of scattering theory is significant. They confirm that the regime of scattering theory is important when the characteristic length a of heterogeneity is smaller than the width L_F of the Fresnel zone. Hence,

$$\frac{L_F}{a} > 1. \tag{17}$$

Moreover, Spetzler & Snieder (2001b) define the width of the central lobe of the sensitivity kernels in Fig. 1 as the width of the Fresnel zone. For a more detailed analysis of the properties of the scattering theoretical sensitivity kernel, we refer to Spetzler & Snieder (2001b).

Sato (1998) (p. 230–238), show how to use the parabolic wave equation to derive the MS-value of phase fluctuations. The parabolic wave equation is based on the assumption that $ak \gg 1$, where k is the wavenumber, thus the regime of ray theory is significant. The MS-value of phase fluctuations Φ^2 in eq. (8.27) of Sato (1998) is valid for a Gaussian random medium in the geometrical optic region that is $Z \gg a \Rightarrow L \gg a$, where Z is the propagation distance and L is the source–receiver distance. Hence, the MS-value of time-shift variations is related to the MS-value of phase fluctuations through

$$\begin{aligned}\langle(\delta t)^2\rangle &= \frac{\Phi^2}{\omega^2} \\ &= \frac{\sqrt{\pi}\varepsilon^2 a k^2 Z}{\omega^2} \\ &= \sqrt{\pi}(\varepsilon u_0)^2 a L,\end{aligned} \tag{18}$$

where ω is the angular frequency, the wave number $k = \omega u_0$ and the propagation distance $Z = L$. The expression for the MS-value of time-shift fluctuations in eq. (18) is identical to the ray theoretical expression in eq. (7). The scattering theoretical approach in the scattering theory section is based on the Rytov approximation (Snieder & Lomax 1996). No assumptions on the wavelength are made in order to derive the scattering theoretical time-shift expression in eq. (9) (see Spetzler & Snieder 2001b). The scattering formulation applied in this study is therefore considered to be a more general solution to the wave equation for which the finite-frequency of waves is taken into account.

3 SETUP OF THE 3-D LABORATORY EXPERIMENT

In order to quantify and substantiate the theoretical aspects discussed in the previous sections, we made use of the experimental results from Sivaji *et al.* (2001). We employed rock samples with various scale length of heterogeneity. The dimensions of the rock samples are $8 \times 30 \times 30$ cm. Elastic waves are produced using a piezo-electric transducer with the driving signal of a single-cycle sine-wave of 500 kHz frequency. See Sivaji *et al.* (2001) or Nishizawa *et al.* (1997) for a sketch of the laboratory experiment. We observe transmitted elastic waves by using a laser Doppler vibrometer. The details of the laser Doppler vibrometer for measuring elastic waves are described in Nishizawa *et al.* (1997, 1998).

Sivaji *et al.* (2001) performed the waveform measurements on a steel block and on granitic rocks from the Westerly and Oshima granites. Photographs of the microstructures of the two granitic rocks are shown in Fig. 2. Waveforms were obtained over a small aperture grid array with a length of 10 mm and spacing of 1 mm. Sivaji *et al.* (2001) found that the scale length of heterogeneity correlates positively with the variance of arrival time or energy fluctuations of the P-wave. In their work, the arrival time of the P-wave is detected as a non-linear change of the waveform.

In this work, however, we use a different method because we determine the traveltime fluctuation as the fluctuation of phase in harmonic waves. We use a Butterworth filter to bandpass-filter the waveforms so that unwanted noise is removed. The central frequency and the bandwidth of the Butterworth filter are determined from the power spectra of the original waveforms; the central frequency is fixed to 500 kHz and the bandwidth is set to 400 kHz. We applied the arrival time of the first clear minimum just after the onset of the P-wave. We corrected the arrival times for slightly different source–receiver distances caused by a grid configuration of observation points. The deviations of the measured arrival times from their mean value are considered time-shifts. The MS-value $\langle(\delta t)^2\rangle$ of time-shift fluctuations is computed by taking the square of the observed

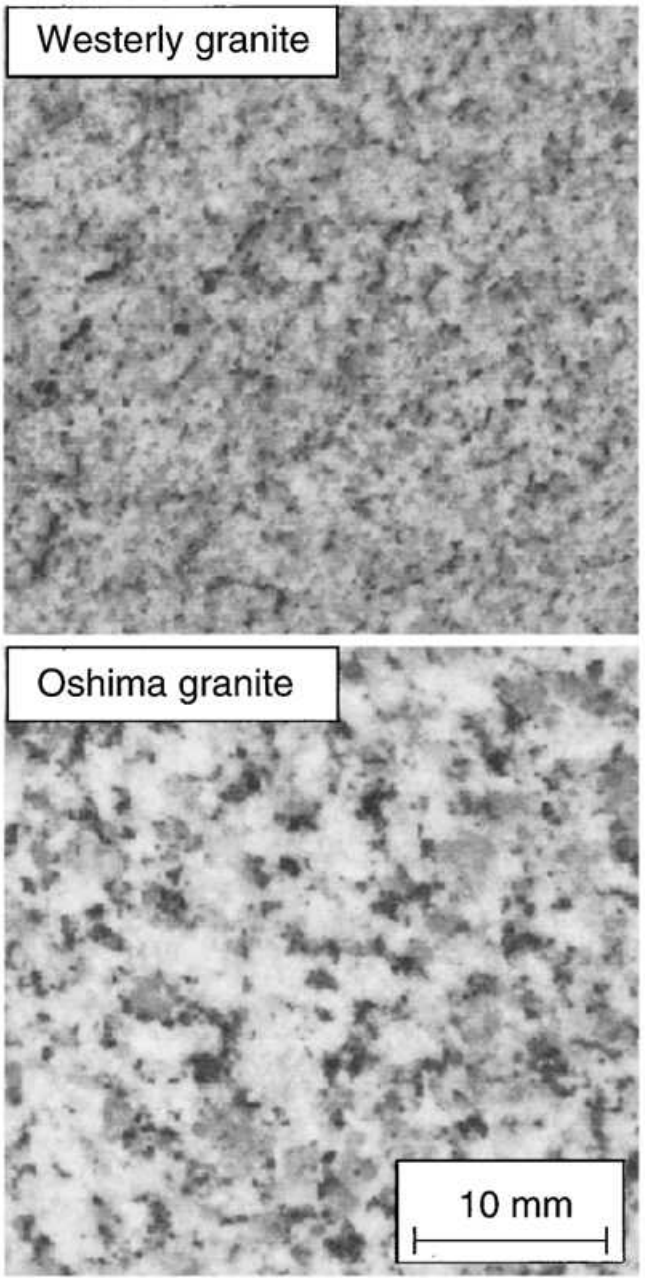

Figure 2. Photograph of the Westerly and Oshima granite which shows the micro-structure of the samples. The three major constituent minerals are biotite (black), quartz (grey) and plagioclase (white).

time-shifts and then calculating the mean value. Hence,

$$\langle(\delta t)^2\rangle = \frac{1}{M}\sum_{i=1}^{M}(\delta t_i)^2, \tag{19}$$

where the integer M is the number of time-shifts in the sample (see Kreyszig 1993). The observed MS-value of time-shift fluctuations for Westerly and Oshima granite is 5.1×10^{-16} and 5.5×10^{-15} s^2, respectively, (see Table 1). In order to evaluate the picking error of the time-shift, we estimated the time-shifts of ultrasonic waves propagating through a homogeneous steel block of the same dimensions. The square root of the MS-value of the time-shift variation for steel, i.e. $\sqrt{\langle(\delta t)^2\rangle}=2.76\times10^{-8}$ s, is defined as the average error of the time-shift picking in the ultrasonic wave experiment. Notice that the square root of the MS-value of the time-shift fluctuations for Westerly granite ($\sqrt{\langle(\delta t)^2\rangle}=2.3\times10^{-8}$ s) is comparable with the root mean squared value of the time-shift variations for steel. Westerly granite can therefore be considered almost homogeneous.

Table 1. The statistical parameters for the exponential auto-correlation function and the MS-value $\langle(\delta t)^2\rangle$ of timeshift variations for Westerly and Oshima granite. The reference velocity is denoted v_0, the rms value of relative slowness pertubations is written as ε and the correlation length is denoted a.

Sample	v_0 (m/s)	ε (%)	a (mm)	$\langle(\delta t)^2\rangle$ (s^2)
Westerly granite	4851.9	8.5	0.22	5.1×10^{-16}
Oshima granite	4644.1	9.4	0.46	5.5×10^{-15}

4 AUTO-CORRELATION FUNCTION FOR WESTERLY AND OSHIMA GRANITE

The major constituent minerals present in Westerly and Oshima granite are biotite, quartz and plagioclase, identified by the black, gray and white areas in the microstructure images, Fig. 2 (Fukushima 2000). The distribution of these minerals is random in space with different grain sizes. The grain size in Westerly granite is small compared to that of Oshima granite.

The characteristics of random media are described by spatial auto-covariance functions of the slowness and density fluctuations, or by their power spectra (Sato 1998). Well-log data are often applied for representing the underground random heterogeneity (Wu *et al.* 1994; Holliger 1996, 1997; Shiomi *et al.* 1997; Goff & Holliger 1999). Since well-log data are sampled against depth with an equal interval, they are considered as continuous data that can easily be converted to the slowness or density fluctuations, and their auto-covariance functions are calculated directly from the data. On the other hand, Holliger & Levander (1992, 1994), Levander *et al.* (1994) and Goff *et al.* (1994) applied discrete data of velocity heterogeneity based on geological maps where the seismic slowness of each rock facies are given by the laboratory-measured seismic slowness.

We have adopted the second methodology to estimate the length-scale of heterogeneity for Westerly and Oshima granite using the digital images of their micro-structure in Fig. 2. We took images of rock surfaces by using a scanner with 600 dpi (dot per inch), and converted the images into tri-modal colour images (Fig. 3a for Oshima granite). The traverse line is set in the tri-mode pattern, and the P-wave slowness values are assigned to each area crossed by the traverse line (see Fig. 3b for the P-wave profiles for Oshima). We assume that quartz and plagioclase are isotropic having the mean velocity calculated from the Voigt–Reuss averages of the elastic parameters of single crystals. The Voigt–Reuss averages give the P-wave slowness $u_{\text{quartz}}=1.527\times10^{-4}$ sm^{-1} for quartz and $u_{\text{plagioclase}}=1.639\times10^{-4}$ sm^{-1} for plagioclase (Simmons & Wang 1971). On the other hand, biotite minerals show strong velocity anisotropy (Aleksandrov & Ryzhova 1961). We assume that the velocity fluctuation of granitic rocks are mostly controlled by the velocity difference between biotite and the other two minerals. For biotite, we select the slowness randomly from the range between the maximum and minimum P-wave slowness

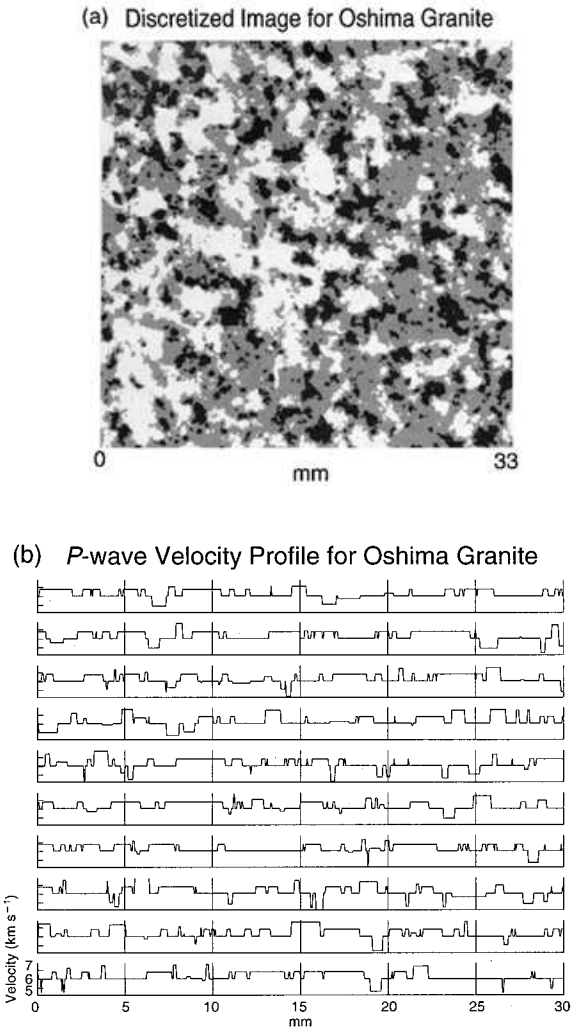

Figure 3. (a) The trimodal-colour image of Oshima granite; white, grey and black colours correspond to plagioclase, quartz and biotite, respectively. (b) 1-D Velocity fluctuation obtained from trimodal-colour image by assuming that the orientation of biotite is random and of the other minerals is isotropic.

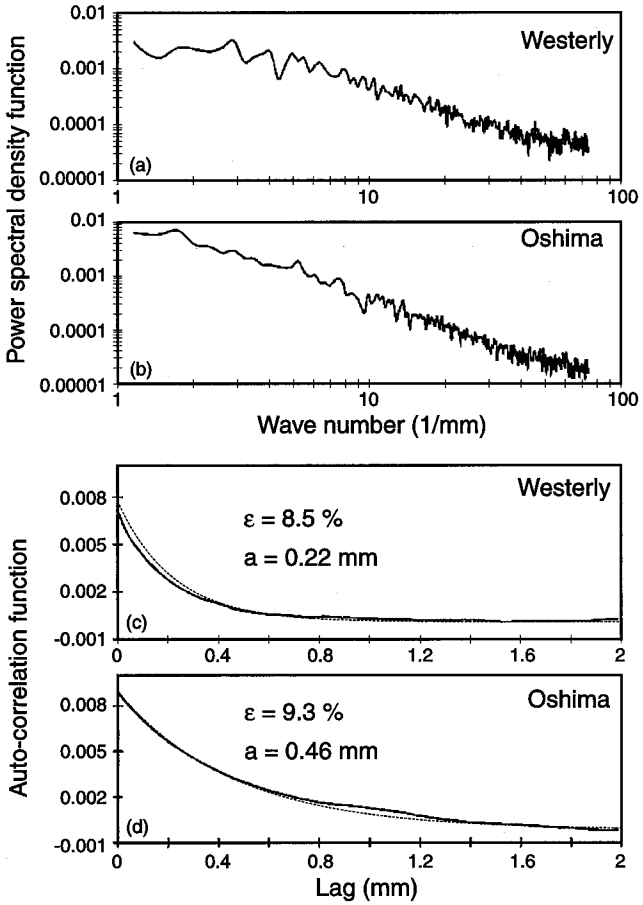

Figure 4. The independent determination of the auto-correlation function which describes statistically the slowness perturbation field of Westerly and Oshima granite. (a) The PSDF for Westerly granite. (b) The PSDF for Oshima granite. (c) The auto-correlation function for Westerly granite and its statistical parameters. (d) The auto-correlation function for Oshima granite and its stochastic parameters. It is found that the best fitting auto-correlation function to the curve in (c) and (d) is exponential. The best fitting exponential auto-correlation functions are shown with the dashed line in (c) and (d).

($u_{\min} = 1.282 \times 10^{-4}$ sm^{-1} and $u_{\max} = 2.375 \times 10^{-4}$ sm^{-1}). The slowness perturbation is then calculated by removing the mean slowness value of the slowness fluctuation in the traverse.

After applying an anti-aliasing filter, the power spectral density function (PSDF) is estimated. This procedure is repeated for 20 profiles and the average PSDF is obtained. The PSDF for Westerly and Oshima are shown in Fig. 4(a) and (b). The auto-covariance function is computed by taking the inverse Fourier transform of the average PSDF. The exponential auto-covariance functions with the best fitting values of the relative slowness perturbation and correlation length are plotted with the dashed line in Fig. 4(c) and (d). The best fitting values for the relative slowness perturbation and correlation length for Westerly and Oshima granite are 8.5 per cent and 0.22 mm, and 9.4 per cent and 0.46 mm, respectively, (Table I). Notice that the characteristic length of heterogeneity for Oshima granite is about twice as large as that for Westerly granite but the strength parameter ε is almost the same indicating that the difference of heterogeneity between the two granitic rocks is characterized by the difference of length-scale of heterogeneity.

It is interesting to note that the measured auto-covariance functions are neither of the Gaussian type nor of the von Karman type. The high frequency limit of PSDF is determined by the image resolution (600 dpi: 0.043 mm). The characteristic scale lengths of heterogeneity are larger than the resolution limit for both Westerly and Oshima granite.

Goff & Holliger (1999) recently found that the heterogeneous structure of most of the crystalline crust can be characterized by the power spectra changing from $1/f$ to $1/f^2$ within the measured frequency range. If this is true, the heterogeneity is self-similar and no characteristic scale of heterogeneity exists. The smooth decay of the PSDF (Fig. 4a and b) of the granitic rocks in the higher frequency is similar to the results found in Goff & Holliger (1999). The characteristic length a corresponds to the longest wave length limit of heterogeneity. The exponential auto-covariance function seems to simulate the real crustal heterogeneity better than other types of auto-covariance functions. Thus, the present experiments may be realistic for simulating real crustal heterogeneity in the shorter wave length regime.

The width of the Fresnel zone is $L_F=\sqrt{\lambda L}\approx 2.7$ cm for both Westerly and Oshima granite using ultrasonic waves with the central frequency equal to 500 kHz ($\lambda=9.7$ mm for Westerly granite and $\lambda=9.3$ mm for Oshima granite) and $L=8$ cm. (The width L_F of the Fresnel zone is derived in Spetzler & Snieder 2001b). By comparing the width of the Fresnel zone with the correlation length for Westerly ($a=0.22$ mm) and Oshima granite ($a=0.46$ mm), we see that the ultrasonic wave laboratory experiment is in the regime of scattering theory according to eq. (17).

5 2-D NUMERICAL EXPERIMENT TO TEST THE STOCHASTIC SCATTERING APPROACH

We use a finite-difference (FD) solution of the acoustic wave equation to test the scattering theory for the statistical measurements of the MS-value of time-shift variations in the real ultrasonic wave experiment. The applied source function is a Ricker wavelet. An incident plane wave is emitted in a 2-D, Cartesian medium and recorded at the source-receiver distance $L=8$ cm. The waveforms measured at the receiver positions are bandpass-filtered between 250 and 1000 kHz. We operate with two slowness fields in the FD-modelling experiment; the reference slowness field which has the constant reference slowness $u_0 = 2.5 \times 10^{-4}$ sm^{-1}, and the perturbed slowness field with the slowness field $u(\mathbf{r})=u_0(\mathbf{r})+u_1(\mathbf{r})$ where $u_1(\mathbf{r})$ is a realization of the exponential or Gaussian quasi-random medium. For both kinds of quasi-random media, we fix the relative slowness perturbation to 3 and 10 per cent, and the correlation length varies between 0.4 and 2 mm. The realizations of the exponential and Gaussian random medium are normalized according to Table I in (Frankel & Clayton 1986).

An example of a numerical simulation of an exponential quasi-random medium using the statistical values (correlation length and the rms value of slowness fluctuations) for Oshima is shown in Fig. 5. There is a close resemblance between Fig. 2b and 5 which indicates that the FD-experiment using quasi-random media simulates the physical laboratory experiment well.

Notice that the mean value of slowness perturbations is not necessarily zero in a finite sampling of a random medium (see Müller *et al.* 1992). We have corrected the realizations of the exponential and Gaussian slowness fields by subtracting each point of the FD-grid with the difference between the mean value of the slowness field sample and the reference slowness u_0. Thereby, each realization of the exponential and Gaussian random media in the numerical experiment has the mean value equal to the reference slowness.

The synthetic time-shifts are obtained by comparing the bandpass-filtered reference waveforms from the constant reference model with the bandpass-filtered perturbed waveforms due to the perturbation models. In Fig. 6, the perturbed seismograms for realizations of the exponential and Gaussian quasi-random media using $a=0.4$, 1 and 2 mm, and $\varepsilon=10$ per cent are shown. The fluctuation of the first arrival increases for increasing value of the correlation length. Similarly, the coda-wave generation is more significant for higher values of the correlation length for both exponential and Gaussian random media. The traveltime of the reference waveform and of the perturbed waveform is determined using the first

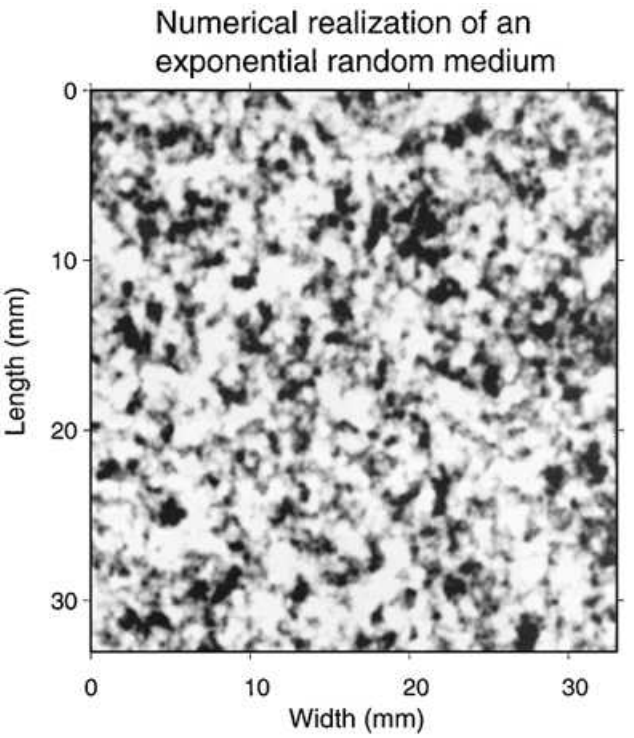

Figure 5. Numerical simulation of the slowness field for Oshima granite. The statistical values for the exponential random medium describing the slowness field of Oshima granite are $a=0.46$ mm and $\varepsilon=9.4$ %.

clear minimum of the waveforms as point of measurement. The FD-time-shift is the difference between the reference and perturbed traveltime. For each distinct correlation length and magnitude of the slowness perturbation field, five realizations of the exponential and Gaussian random media with different random seed number are used to generate the FD-time-shifts. For each realization of the random media, 150 time-shifts are measured in the FD-experiment. Given the correlation length and magnitude of the slowness perturbation field for either the exponential media or the Gaussian random media, the MS-value of the sample of the FD-time-shift fluctuations for every realization is calculated with eq. (19). It gives five MS-values of time-shift fluctuations, $\langle(\delta t)^2\rangle_j$, where $j=1,\ldots 5$, for each combination of the correlation length and the rms value of relative slowness perturbations for the exponential random media and the Gaussian random media. The average value $\langle(\delta t)^2\rangle_{ave}$ of the sample of MS-values of FD-time-shifts for each set of the correlation length and the rms value of relative slowness perturbation fields is computed as

$$\langle(\delta t)^2\rangle_{ave} = \frac{1}{N}\sum_{j=1}^{N}\langle(\delta t)^2\rangle_j, \tag{20}$$

The standard deviation $\sigma(\langle(\delta t)^2\rangle)$ of the sample of MS-values of FD-time-shift variations for each combination of the correlation length and the rms value of the relative slowness perturbation field is given by

$$\sigma^2(\langle(\delta t)^2\rangle) = \frac{1}{N-1}\sum_{j=1}^{N}\left(\langle(\delta t)^2\rangle_j - \langle(\delta t)^2\rangle_{ave}\right)^2, \tag{21}$$

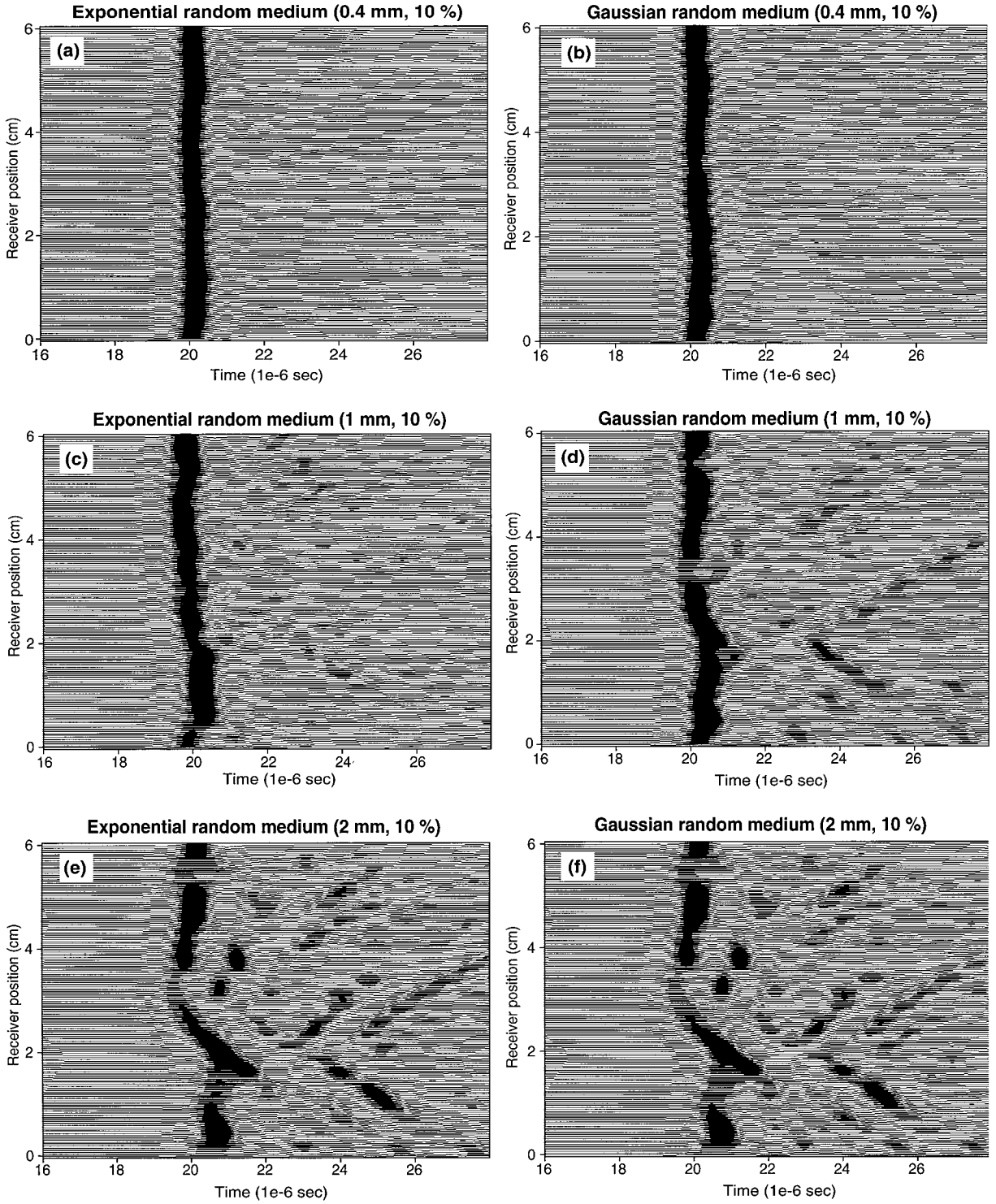

Figure 6. Synthetic seismograms from the FD-simulation of the laboratory experiment using different realizations of an exponential quasi-random medium and a Gaussian quasi-random medium with the reference slowness $u_0 = 2.5 \times 10^{-4}$ sm^{-1} and the relative slowness perturbation $\varepsilon = 10$ per cent. (a) Exponential quasi-random medium with $a = 0.4$ mm, (b) Gaussian quasi-random medium with $a = 0.4$ mm, (c) Exponential quasi-random medium with $a = 1$ mm, (d) Gaussian quasi-random medium with $a = 1$ mm, (e) Exponential quasi-random medium with $a = 2$ mm, (f) Gaussian quasi-random medium with $a = 2$ mm.

(see Kreyszig 1993). The standard deviation of the sample of the MS-values for FD-time-shifts is defined as the observed error in the estimation of the MS-value of FD-time-shifts.

In order to compute the scattering theoretical MS-value of time-shift fluctuations in eq. (10) for exponential and Gaussian random media in the FD-experiment, we must use the 2-D

sensitivity kernel for a plane wave due to diffraction theory, hence

$$K(x, z) = \sqrt{u_0} \int_{v_0-\Delta v}^{v_0+\Delta v} A(v)\sqrt{v}\, \frac{\sin\left(\pi v u_0 \dfrac{z^2}{(L-x)} + \dfrac{\pi}{4}\right)}{\sqrt{L-x}}\, dv. \quad (22)$$

which is explicitly derived in Spetzler & Snieder (2001b). The ray theoretical MS-value of time-shift fluctuations is calculated with eq. (4) wherein the exponential and Gaussian auto-covariance function is inserted.

The width of the Fresnel zone due to a plane wave is about $L_F = \sqrt{3\lambda L} = 3.9$ cm (Spetzler & Snieder 2001b) for $L = 8$ cm and $\lambda = 1/(u_0 v_0) = 6.4$ mm. According to eq. (17), we are in the regime of scattering theory using the correlation length $a = 0.4 - 2$ mm in the numerical experiment.

6 RESULTS

In this section, we present the statistical measurements of the MS-values of time-shift fluctuations from the laboratory experiment and from the FD-numerical experiment. In Fig. 7, the theoretical MS-value of time-shift fluctuations for different correlation lengths between 0.15 and 0.55 mm are computed using ray theory (dotted line) in eq. (4) and 3-D scattering theory (dashed line) in eq. (10) for the exponential random medium in the laboratory experiment. Notice that a logarithmic scale is used for the y-axis. The reference slowness and relative slowness perturbation given in Table 1 for Oshima granite were applied as statistical model parameters in the exponential auto-covariance function for the two granite samples. The observed

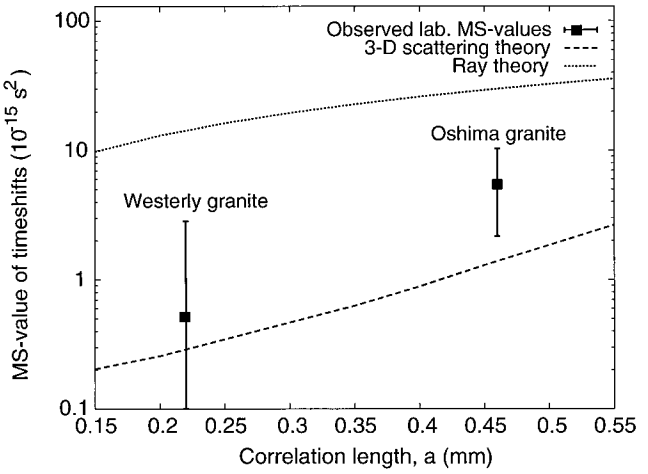

Figure 7. The MS-value of time-shift fluctuations versus the correlation length computed with ray theory (dotted line) and 3-D scattering theory (dashed line) for the exponential random medium in the ultrasonic wave experiment. The offset $L = 8$ cm, the slowness $u_0 = 2.153 \times 10^{-4}$ sm^{-1} and the relative slowness perturbation $\varepsilon = 9.4$ per cent for Oshima granite. The observed MS-value of time-shift fluctuations from the laboratory experiment is plotted at the correlation length $a = 0.22$ mm (Westerly) and 0.46 mm (Oshima) with points and errorbars. We see that scattering theory predicts the observed MS-value of time-shift fluctuations obtained from Westerly granite (within the errorbars) and Oshima granite (just below the errorbar), while ray theory overestimates the observed MS-values of time-shift variations in the laboratory experiment.

MS-value of time-shift perturbations for Westerly ($a = 0.22$ mm) and Oshima ($a = 0.46$ mm) granite is shown with points and error bars. The size of the error bars for the MS-value of time-shifts for Westerly and Oshima granites indicates the picking error of the time-shifts in the ultrasonic wave experiment. Westerly granite has a slightly different reference slowness and rms value of relative slowness fluctuations than Oshima granite so the observed MS-value of time-shift fluctuations for Westerly granite in Fig. 7 has been corrected by multiplying with the factor $(u_0^{Osh}\varepsilon^{Osh})^2/(u_0^{West}\varepsilon^{West})^2 = 1.33$. We see in Fig. 7 that ray theory overestimates the observed MS-values of time-shift fluctuations for Westerly and Oshima granite. The MS-value of time-shift variations computed with scattering theory is inside the error bars of the observed statistical value for Westerly granite and a bit below the error bar of the observed MS-value for time-shifts for Oshima granite. However, the MS-values of time-shifts that take the scattering of waves into account are in the same order of magnitude as the observed statistical values for the Westerly and Oshima granites, while the MS-values of time-shift fluctuations computed with ray theory are a factor 10–15 larger than the stochastic values observed in the ultrasonic wave experiment.

We have simulated the ultrasonic wave experiment with a 2-D numerical experiment which is explained in details in Section 5. The MS-values of time-shift fluctuations for an exponential and Gaussian quasi-random medium are shown in Fig. 8. The MS-values of time-shift variations computed with ray theory and 2-D scattering theory are shown with the dotted line and dashed line, respectively, while the numerically observed MS-values of time-shift fluctuations for several correlations length are plotted with points and error bars. In Fig. 8(a) (exponential quasi-random medium) and (b) (Gaussian quasi-random medium), the relative slowness perturbation $\varepsilon = 3$ per cent. In Fig. 8(c) (exponential quasi-random medium) and (d) (Gaussian quasi-random medium), $\varepsilon = 10$ %. It is seen that 2-D scattering theory predicts the numerically observed MS-values of time-shift perturbations within the error bars, while the ray theoretical MS-values of time-shift variations are generally too large.

We show in Figs 9 and 10 that 2-D scattering theory (dashed line) is much more accurate than ray theory (dotted line) to predict the FD-time-shifts (solid line) using deterministic realizations of exponential and Gaussian quasi-random media with correlations length smaller in size than the width of the Fresnel zone. The ray theoretical time-shift is calculated with eq. (3) and the time-shift due to scattering theory is computed with eq. (9) using the 2-D sensitivity kernel for a plane wave in eq. (22). For the realizations of exponential quasi-random media and Gaussian quasi-random media with $\varepsilon = 10$ % in Figs 9 and 10, respectively, the correlation length $a = 0.4$, 1 and 2 mm which corresponds to the points for which the numerically observed MS-values of time-shift fluctuations in Fig. 8 are computed. In all the figures with the time-shift fluctuations obtained from deterministic realizations of exponential and Gaussian quasi-random media, it is observed that the scattering theoretical time-shift fit the FD-time-shift quite well while ray theory often overestimates or predicts time-shifts out of phase with the FD-time-shifts.

The MS-value of time-shift fluctuations in Figs 7 and 8 and the time-shifts in Figs 9 and 10 are calculated using first order ray perturbation theory, thus principally we only show that ray theory based on Fermat's principle does not hold in the laboratory experiment and the FD-experiment. The effect of

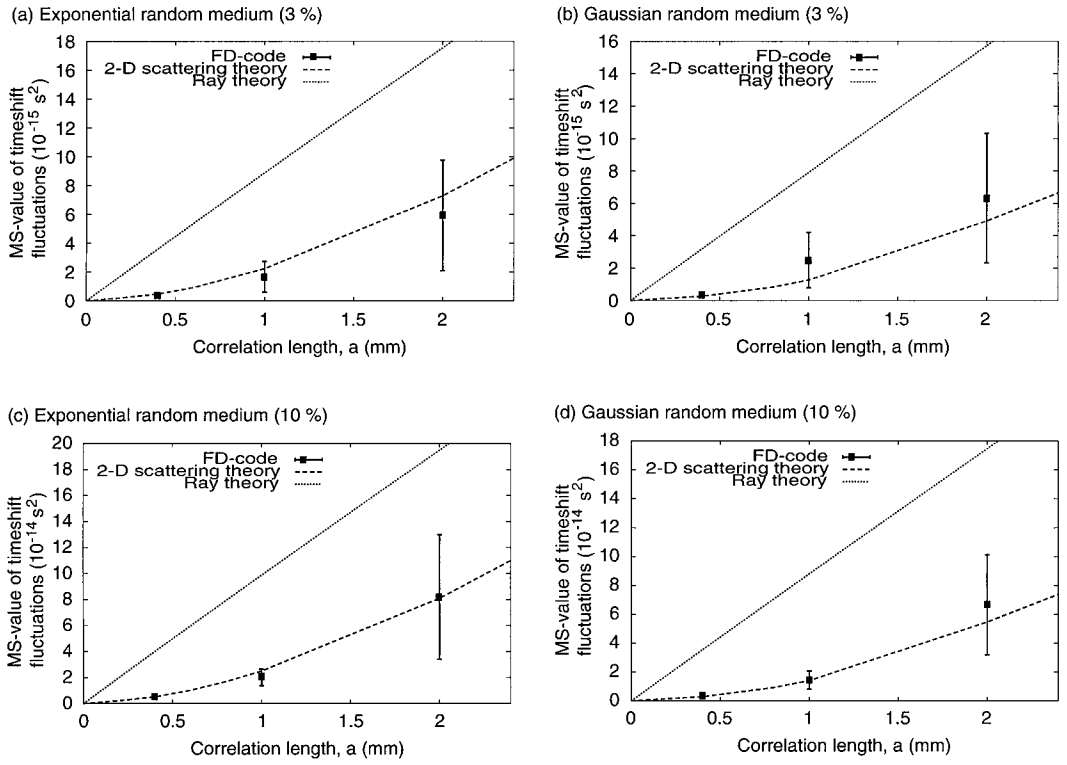

Figure 8. MS-values of time-shift fluctuations for exponential and Gaussian random media with different correlation lengths in the FD-experiment. The reference slowness is 2.5×10^{-4} sm^{-1}, the source-receiver offset is 8 cm for an incident plane wave and the frequency-range is from 250 to 1000 kHz. The MS-value of time-shift fluctuations for ray theory is plotted with the dotted line and for scattering theory with the dashed line. The numerical data are computed for the correlation length which is between 0.4 and 2 mm. The error bars show the standard deviation of the numerically observed measurements. (a) The exponential random medium with the relative slowness perturbation $\varepsilon = 3$ per cent. (b) The Gaussian random medium with $\varepsilon = 3$ per cent. (c) The exponential random medium with $\varepsilon = 10$ per cent. (d) The Gaussian random medium $\varepsilon = 10$ per cent. Scattering theory for waves propagating in 2-D is better than ray theory to predict the observed MS-values of time-shift fluctuations computed in the numerical experiment.

ray bending in Gaussian random media has been investigated by Spetzler & Snieder (2001b). They apply second order ray perturbation theory, thereby including the bending of rays in the calculation of the time-shift due to the perturbation of the slowness medium. Spetzler & Snieder (2001b) find that ray bending effects are not important in Gaussian random media when the Fresnel zone is larger than the correlation length of the realization of the Gaussian random model. The result of Spetzler & Snieder (2001b) also holds for the results from the laboratory experiment and FD-experiment in this study.

7 DISCUSSION

The results of this study has serious implications for seismic exploration and seismology. In Table 2 we present the characteristic values for the wavelength λ, the length L of the ray path between the source and receiver, the width L_F of the Fresnel zone and the length-scale a of slowness anomalies found in present-day tomographic inversions in seismic exploration and seismology. For reference, see Parra & Bangs (1992) for vertical seismic profiling tomography (VSP), Goudswaard *et al.* (1998)

Table 2. Characteristic values of wave experiments in seismic exploration and seismology. The wavelength is denoted λ, the length of the ray path between the source and receiver is L, the length-scale of observed slowness anomalies is a and the width of the Fresnel zone is written as L_F. The following abbreviations are used; VSP: vertical seismic profiling, CT: crosswell tomography, RS: reflection seismic, RSWT: regional surface wave tomography, GSWT: global surface wave tomography and GBWT: global body wave tomography.

	λ	L	L_F	a
VSP	5–250 m	300 m	38–274 m	10–15 m
CT	2–10 m	500 m	32–70 m	5–10 m
RS	80 m	200 m (shallow)–8 km (deep)	126–800 m	25–50 m
RSWT	450 km	1–70 deg	200–1735 km	1000 km
GSWT	450 km	20–160 deg	870–4940 km	3000–4000 km
GBWT	6 km	100–20000 km	25–346 km	50–100 km

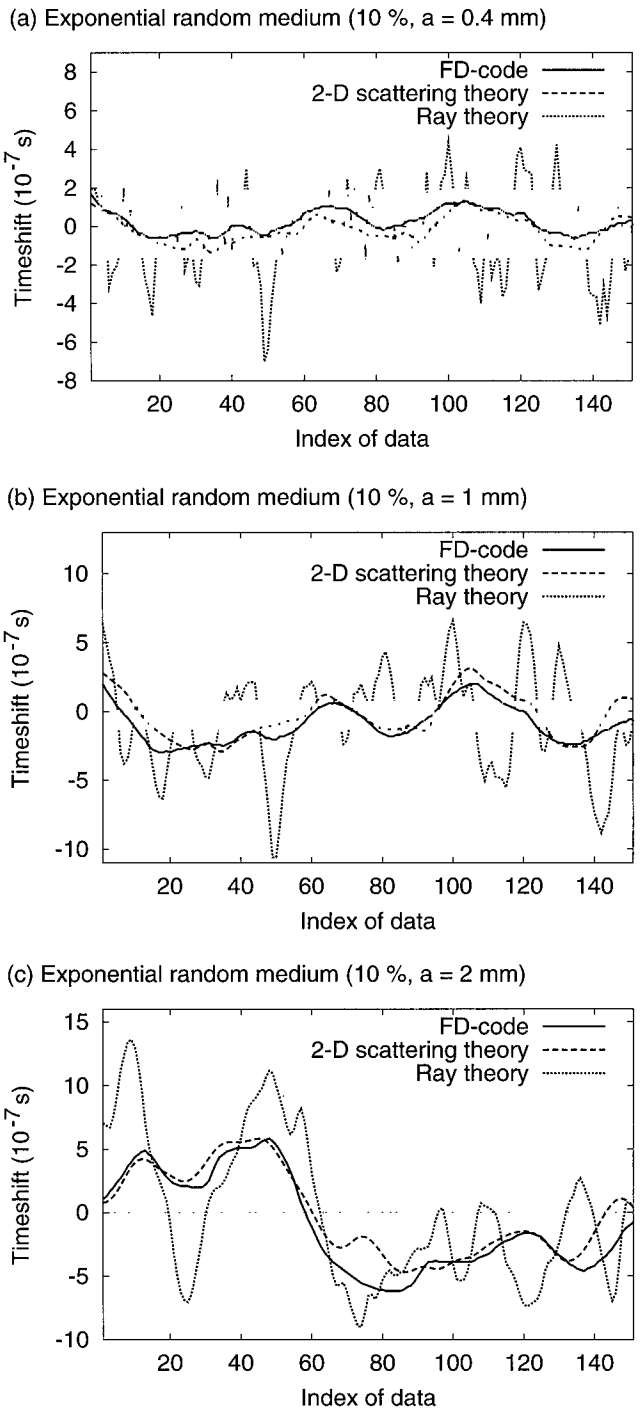

Figure 9. Time-shifts obtained from ray theory, 2-D scattering theory and the FD-solution of the wave equation for different realizations of an exponential quasi-random medium with the reference slowness $u_0 = 2.5 \times 10^{-4}$ s m^{-1} and the relative slowness perturbation $\varepsilon = 10$ per cent. The source-receiver offset $L = 8$ cm for an incident plane wave. The measured waveforms are bandpass-filtered in the frequency-range from 250 to 1000 kHz. (a) The correlation length $a = 0.4$ mm, (b) $a = 1$ mm and (c) $a = 2$ mm.

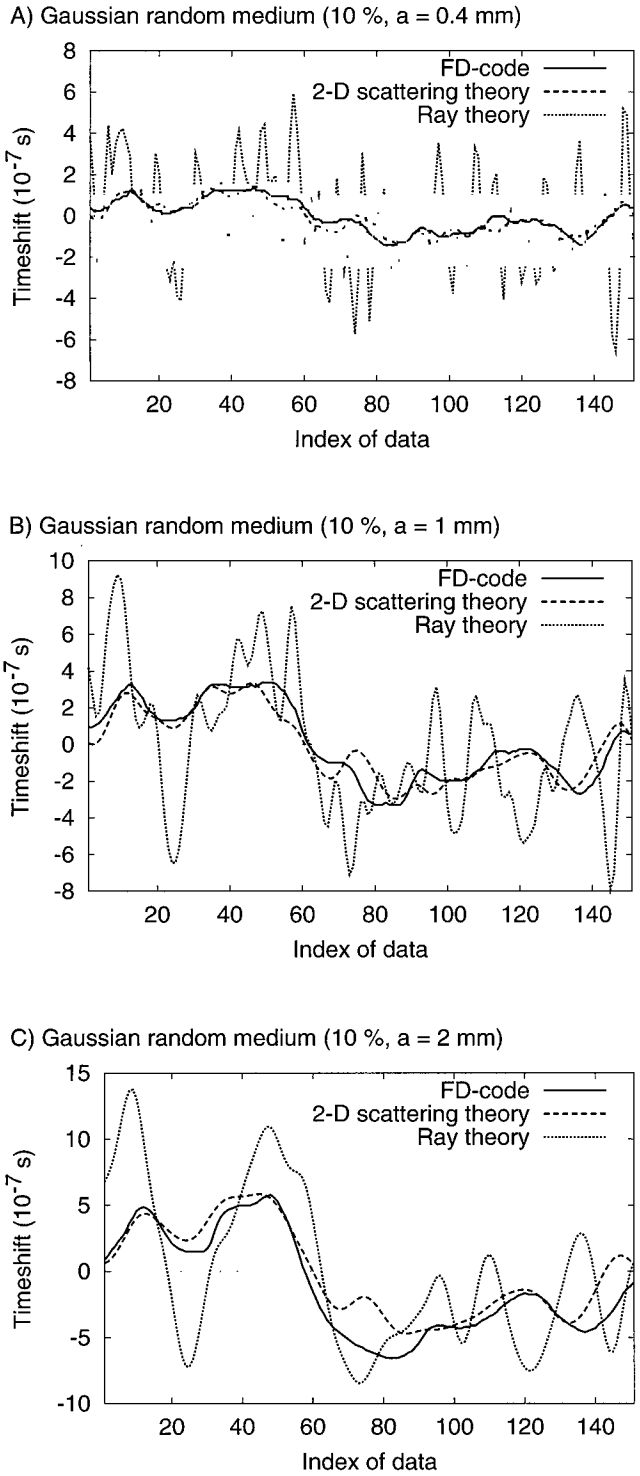

Figure 10. As in Fig. 9, but using different realizations of the Gaussian quasi-random medium with the relative slowness perturbation $\varepsilon = 10$ per cent. (a) The correlation length $a = 0.4$ mm, (b) $a = 1$ mm and (c) $a = 2$ mm.

for crosswell tomography (CT), Hatchell (2000) for reflection seismic (RS), van der Lee & Nolet (1997) for regional surface wave tomography (RSWT), Trampert & Woodhouse (1995) for global surface wave tomography (GSWT) and Bijwaard & Sparkman (1998) for global body wave tomography (GBWT). For 3-D wave propagation experiments that is VSP, CT and GBWT, the maximum width of the Fresnel zone is given by

$$L_F = \sqrt{\lambda L}, \tag{23}$$

(Spetzler & Snieder 2001b) and for RS, the maximum width of the Fresnel zone at the reflector is as well given by eq. (23) but the parameter L is then the two-way length of the wave path from the source to the reflector and back to the receiver. Surface wave tomography (e.g. RSWT and GSWT) is a 2-D wave propagation experiment, so the maximum width of the Fresnel zone on the sphere is given by

$$L_F = \sqrt{\frac{3R\lambda}{2}\tan\left(\frac{L}{2}\right)}, \tag{24}$$

where R is the radius of the Earth, and the epicentral distance L is in radians, (see eq. 35 in Spetzler & Snieder 2001b). By comparing the width of the Fresnel zone with the characteristic length of inhomogeneity for the different wave experiments in Table 2, we see that the regime of scattering theory is important according to eq. (17) in most of the tomographic experiments under consideration.

8 CONCLUSIONS

We have shown evidence that scattering theory is more accurate than ray theory to predict time-shifts for media with length-scales of inhomogeneity smaller in size than the width of the Fresnel zone. We used a stochastic approach to compute the MS-value of time-shift variations using ray theory and scattering theory because the slowness perturbation field of Westerly and Oshima granites used in the laboratory experiment could be described rather well as an exponential random medium. We compared the MS-value of the observed time-shift distribution for Westerly and Oshima granites in the ultrasonic wave experiment with those calculated theoretically with ray and scattering theory wherein the statistical parameters for the two granite samples were applied. Interestingly, we saw that ray theory would predict too large MS-values of time-shift variations, while scattering theory gave well-fitting values which are close to the observed MS-values of time-shift fluctuations for the Westerly and Oshima granites. The result of the laboratory experiment was simulated with a numerical FD-experiment using small-scale structured random media. In the numerical experiment, we showed that scattering theory is better than ray theory to fit both the MS-value of FD-time-shifts from different stochastic models and the FD-time delays measured in deterministic realizations of the random media.

Present-day tomographic models in seismic exploration and seismology are at the edge to explore Earth models with structures smaller than the width of the Fresnel zone. It is therefore necessary to incorporate the finite-frequency effect of waves in seismic reconstruction techniques so that we can get more reliable small-scale models of the Earth. In addition, the applied scattering theory in this paper is a linear theory which makes it just as easy to apply as ray theory. It is therefore feasible in the near-future to incorporate the non-ray geometrical effect into tomographic imaging techniques.

ACKNOWLEDGMENTS

We gratefully thank the Danish Oil Company, Dansk Olie og Naturgas Selskab (DONG) for the jubilee scholarship to JS. Without this bursary he would not have been able to visit Sivaji and Nishizawa-san at Geological Survey of Japan in Tsukuba where the real measurements using ultrasonic waves were done. We would also like to thank Roel Snieder for his comments and advices in order to improve the manuscript. The two reviewers Klaus Holliger and Ulrich Wegler showed much interest in this study, and their remarks helped us to clarify many important points in the paper. The investigations were (in part) supported by *the Netherlands Geosciences Foundation* (GOA) with financial aid from *the Netherlands Organisation for Scientific Research* (NWO) through the project 750.297.02.

REFERENCES

Abramowitz, M. & Stegun, I.A., 1970. *Handbook of Mathematical Functions with Formulas, Graphs and Mathematical Tables,* Dover Publications, Inc., New York.

Aleksandrov, K.S. & Ryzhova, T.V., 1961. The elastic properties of rock-forming minerals, II: Layered silicates, *Izv. Acad. Sci. USSR, Geophys. Ser. 12,* 186–189.

Bijwaard, H. & Spakman, W., 1998. Closing the gap between regional and global travel time tomography, *Geophys. Res. Lett.,* **103,** 30 055–30 078.

Bleistein, N., 1984. *Mathematical Methods for Wave Phenomena,* Academic Press, Orlando.

Curtis, A., Trampert, J., Snieder, R. & Dost, B., 1998. Eurasian fundamental mode surface wave phase velocities and their relationship with tectonic structures, *J. geophys. Res.,* **103,** 26919–26947.

Dahlen, A., Hung, S.H. & Nolet, G., 2000. Fréchet Kernels for finite-frequency traveltimes I. Theory, *Geophys. J. Int.,* **141,** 157–174.

Dubendorff, B. & Menke, W., 1986. Time-domain apparent-attenuation operators for compressional and shear waves: experiment versus single-scattering, *J. geophys. Res.,* **91,** 14 023–14 032.

Frankel, A., Clayton, R.W., 1986. Finite difference simulations of seismic scattering: Implication for the propagation of short-period waves in the crust and models of crustal heterogeneity, *J. geophys. Res.,* **91,** 6465–6489.

Fukushima, Y., 2000. Laboratory study on scattering characteristics of shear Waves in rock samples, *M.Sc thesis,* Tohoku University, Sendai.

Goff, J.A., Holliger, K. & Levander, A., 1994. Model fields: A new method for characterization of random seismic velocity Heterogeneity, *Geophys. Res. Lett.,* **21,** 493–496.

Goff, J.A. & Holliger, K., 1999. Nature and origin of upper crustal velocity fluctuations and associated scaling properties: combined stochatic analyses of KTB velocity and lithology logs, *J. geophys. Res.,* **104,** 13 169–13 182.

Goudswaard, J.C.M., ten Kroode, F.P.E., Sneider, R. & Verdel, A.R., 1998. Detection of lateral velocity contrasts by crosswell travel time tomography, *Geophysics,* **63,** 523–533.

Hatchell, P.K., 2000. Fault whispers: transmission distortions on prestack seismic reflection data, *Geophysics,* **65,** 377–389.

Holliger, K. & Levander, A., 1992. A stochastic view of lower crustal fabric based on evidence from the Ivrea zone, *Geophys. Res. Lett.,* **19,** 1153–1156.

Holliger, K. & Levander, A., 1994. Seismic structure of gneissic/granite upper crust: geological and petrophysical evidence from the Strone-Ceneri Zone (Nothern Italy) and implications for crustal seismic exploration, *Geophys. J. Int.,* **119,** 497–510.

Holliger, K., 1996. Seismic velocity heterogeneity of the upper crystalline crust as derived from a variety of *P*-wave sonic logs, *Geophys. J. Int.,* **125,** 813–829.

Holliger, K., 1997. Seismic scattering in the upper crystalline crust based on evidence from sonic logs, *Geophys. J. Int.,* **127,** 65–72.

Hung, S.H., Dahlen, A. & Nolet, G., 2000. Fréchet Kernels for finite-frequency traveltimes II. Examples, *Geophys. J. Int.,* **141,** 175–203.

Kreyszig, E., 1993. *Advanced Engineering Mathematics,* John Wiley & Sons, Chichester.

van der Lee, S. & Nolet, G., 1997. Upper mantle *S*-velocity structure of North America, *J. geophys. Res.*, **102,** 22 815–22 838.
Levander, A., England, W., Smith, S.K., Hobbs, R.W., Goff, J.A. & Holliger, K., 1994. Stochastic characterisation and seismic response of upper and middle crustal rocks based on the Lewisian Gneiss Complex, Scotland, *Geophys. J. Int.*, **119,** 243–259.
Lo, T., Toksöz, M.N., Xu, S., Wu, R., 1988. Ultrasonic laboratory tests of geophysical tomographic reconstruction, *Geophysics,* **53,** 947–956.
Marquering, H., Nolet, G., Dahlen, F.A., 1998. Three-dimensional waveform sensitivity kernels, *Geophys. J. Int.*, **132,** 521–534.
Marquering, H., Dahlen, F.A. & Nolet, G., 1999. The body-wave travel-time paradox: bananas, doughnuts and 3-D delay-time kernels, *Geophys. J. Int.*, **137,** 805–815.
Matsunami, K., 1991. Laboratory tests of excitation and attenuation of coda waves using 2-D models of scattered media, *Phys. Earth planet. Inter.*, **67,** 36–47.
Menke, W. & Abbot, D., 1990. *Geophysical Theory,* Columbia University Press, New York.
Müller, G., Roth, M. & Korn, M., 1992. Seismic-wave traveltimes in random media, *Geophys. J. Int.*, **110,** 29–41.
Nishizawa, O., Satoh, T., Lei, X. & Kuwahara, Y., 1997. Laboratory studies of seismic wave propagation in inhomogeneous media using a laser doppler vibrometer, *Bull. seism. Soc. Am.*, **87,** 809–823.
Nishizawa, O., Satoh, T. & Lei, X., 1998. Detection of shear waves in ultrasonic range by using a laser doppler vibrometer, *Rev. Sci. Instr.*, **69,** 1–2.
Parra, J.O. & Bangs, J.H., 1992. High-Resolution reverse VSP and interwell seismic experiments at the Buckhorn Test Site in Illinois, *62nd Ann. Int. Mtg., Soc. Expl. Geophys., Exp. Abs.*, 103–107.
Roth, M., Müller, G. & Snieder, R., 1993. Velocity shift in random media, *Geophys. J. Int.*, **115,** 552–563.
Roth, M., 1997. Statistical interpretation of travel time fluctuations, *Phys Earth Planet. Inter.*, **104,** 213–225.
Sato, H. & Fehler, M., 1998. *Seismic Wave Propagation and Scattering in the Heterogeneous Earth,* Springer Verlag, New York.
Schultz, C.H. & Toksöz, M.N., 1993. Enhanced backscattering of seismic waves from a highly irregular interface: *SH* case, *Geophys. J. Int.*, **114,** 91–102.
Schultz, C.H. & Toksöz, M.N., 1994. Enhanced backscattering of seismic waves from a highly irregular interface: *P-SV* case, *Geophys. J. Int.*, **117,** 783–810.
Schultz, C.H. & Toksöz, M.N., 1995. Reflections from a randomly grooved interface: ultrasonic modelling and finite-difference calculation, *Geophys. Prospect.*, **43,** 581–594.
Shiomi, K., Sato, H. & Ohtake, M., 1997. Broad-band power-law spectra of well-log data in Japan, *Geophys. J. Int.*, **130,** 57–64.
Simmons, G. & Wang, H., 1971. *Single Crystal Elastic Constants and Calculated Aggregate Properties,* Handbook 2nd Ed. MIT Press, Cambridge.
Sivaji, C., Nishizawa, O. & Fukushima, Y., 2001. Relationship between fluctuations of arrival time and energy of seismic waves and scale-length of heterogeneity: an inference from experimental study, *Bull. seism. Soc. Am.*, **91,** 292–303.
Snieder, R. & Sambridge, A., 1992. Ray perturbation theory for traveltimes and ray paths in 3-D heterogeneous media, *Geophys. J. Int.*, **109,** 294–322.
Snieder, R. & Lomax, A., 1996. Wavefield smoothing and the effect of rough velocity perturbations on arrival times and amplitudes, *Geophys. J. Int.*, **125,** 796–812.
Spetzler, J. & Snieder, R., 2001a. The formation of caustics in two and three dimensional media, *Geophys. J. Int.*, **144,** 175–182.
Spetzler, J. & Snieder, R., 2001b. The effects of small-scale heterogeneity on the arrival time of waves, *Geophys. J. Int.*, **145,** 786–796.
Tong, J., Dahlen, F.A., Nolet, G. & Marquering, H., 1998. Diffraction effects upon finite-frequency travel times: a simple 2-D example, *Geophys. Res. Lett.*, **25,** 1983–1986.
Trampert, J. & Woodhouse, J.H., 1995. Global phase velocity maps of love and rayleigh waves between 40 and 150 seconds, *Geophys. J. Int.*, **122,** 675–690.
Yomogida, K. & Aki, K., 1987. Amplitude and phase data inversion for phase velocity anomalies in the Pacific Ocean Basin, *Geophys. J. R. astr. Soc.*, **88,** 161–204.
Yomogida, K., 1992. Fresnel Zone inversion for lateral heterogeneities in the Earth, *Pure appl. Geophys.*, **138,** 391–406.
Vinogradov, S.D., Troitsky, P.A. & Solovyeva, M.S., 1989. Influence of fracturing and stresses on the propagation of elastic waves, *Izvestiya Earth Physics,* **25,** 293–303.
Vinogradov, S.D., Troitsky, P.A. & Solovyeva, M.S., 1992. Study of propagation of elastic waves in medium with oriented cracks, *Izvestiya Earth Physics,* **28,** 367–383.
Woodward, M.J., 1992. Wave-equation tomography, *Geophysics,* **57,** 15–26.
Wu, R.S., Xu, Z. & Li, X.P., 1994. Heterogeneity spectrum and scale-anisotropy in the upper crust revealed by the German Continental Deep-Drilling (KTB) Holes, *Geophys. Res. Lett.*, **21,** 911–914.
Zhao, L., Jordan, T.H. & Chapman, C.H., 2000. Three-dimensional Fréchet differential kernels for seismic delay times, *Geophys. J. Int.*, **141,** 558–576.

APPENDIX A: ANALYTICAL INTEGRATION OVER A CONSTANT FREQUENCY-BAND

To derive the analytical solution of the 2-D scattering sensitivity kernel in eq. (12), we use that the integration of the functional $\sqrt{v}\sin(bv+\pi/4)$ is given by

$$\int \sqrt{v}\sin\left(bv+\frac{\pi}{4}\right)dv = \frac{\sqrt{v}}{\sqrt{2}b}\Big(\sin(bv)-\cos(bv)\Big) + \frac{\sqrt{\frac{\pi}{4}}}{b^{3/2}}\left(C\left(\sqrt{\frac{2bv}{\pi}}\right)-S\left(\sqrt{\frac{2bv}{x}\pi}\right)\right), \tag{A1}$$

where the functions C and S are the Fresnel cosine integral and sine integral, respectively. See Abramowitz & Stegun (1970) for a description of the Fresnel cosine and sine integrals. For the 3-D sensitivity kernel due to non-ray geometrical effects in eq. (14), an integration of the functional $v\sin(bv)$ gives that

$$\int v\sin(bv)dv = -\frac{v\cos(bv)}{b}+\frac{\sin(bv)}{b^2}. \tag{A2}$$

APPENDIX B: THE MS-VALUE OF TIME-SHIFT FLUCTUATIONS USING SCATTERING THEORY IN A HOMOGENEOUS SLOWNESS PERTURBATION MEDIUM

We derive eq. (15) explicitly for 2-D scattering theory. The source–receiver distance is assumed to be much smaller than the correlation length which allows us to set the exponential function in eq. (1) for exponential random media and in eq. (2) for Gaussian random media to unity. The MS-value of time-shifts fluctuations is then derived by rewriting eq. (10) as a

multiplication of two time-shifts, thus

$$\begin{aligned}\langle(\delta t)^2\rangle(L) &= (\varepsilon u_0)^2 \int_0^L \int_0^L \int_{-\infty}^{\infty} \int_{-\infty}^{\infty} K(x', z')K(x'', z'')dx'dz'dx''dz'' \\ &= (\varepsilon u_0)^2 \int_0^L \int_{-\infty}^{\infty} K(x', z')dx'dz' \int_0^L \int_{-\infty}^{\infty} K(x'', z'')dx''dz'' \\ &= (\varepsilon u_0 L)^2, \end{aligned} \tag{B1}$$

because each scattering theoretical sensitivity kernel integrated over the 2-D volume between the source and receiver is equal to the source-receiver offset L as shown below in eq. (B2). Hence

$$\begin{aligned}&\int_0^L \int_{-\infty}^{\infty} K(x, z)dzdx \\ &= \sqrt{u_0 L} \int_{v_0-\Delta v}^{v_0+\Delta v} A(v)\sqrt{v} \int_0^L \frac{1}{\sqrt{x(L-x)}} \\ &\quad \times \int_{-\infty}^{\infty} \sin\left(v\pi u_0 L \frac{z^2}{x(L-x)} + \frac{\pi}{4}\right) dzdxdv \\ &= \frac{\sqrt{u_0 L}}{2i} \int_{v_0-\Delta v}^{v_0+\Delta v} A(v)\sqrt{v} \int_0^L \frac{1}{\sqrt{x(L-x)}} \\ &\quad \times \int_{-\infty}^{\infty} \left(e^{i\left(v\pi u_0 L \frac{z^2}{x(L-x)} + \frac{\pi}{4}\right)} - e^{-i\left(v\pi u_0 L \frac{z^2}{x(L-x)} + \frac{\pi}{4}\right)}\right) dzdxdv \\ &\approx \frac{\sqrt{u_0 L}}{2i} \int_{v_0-\Delta v}^{v_0+\Delta v} A(v)\sqrt{v} \int_0^L \frac{1}{\sqrt{x(L-x)}} \left(2i\sqrt{\frac{x(L-x)}{v u_0 L}}\right) dxdv \\ &= \int_{v_0-\Delta v}^{v_0+\Delta v} A(v)dv \int_0^L dx = L. \end{aligned} \tag{B2}$$

Stationary phase theory (Bleistein 1984) is applied to evaluate the integration of the variable z between $-\infty$ and ∞. A similar derivation holds for 3-D scattering theory for a point source and for the 2-D diffraction sensitivity kernel for a plane wave.

APPENDIX C: THE CONVERGING OF THE MS-VALUE OF TIME-SHIFT FLUCTUATIONS TOWARDS ZERO WHEN THE CORRELATION LENGTH GOES TO ZERO

In this appendix, eq. (16) is derived explicitly for 2-D scattering theory. A similar derivation is valid for the scattering of waves propagating in 3-D. The following integration technique can also be found in Roth *et al.* (1993) and in Spetzler & Snieder (2001a). Let

$$f(r) = \langle \delta u(x', z')\delta u(x'', z'')\rangle, \tag{C1}$$

and

$$\eta(x', x'', z', z'') = K(x', z')K(x'', z''). \tag{C2}$$

The MS-value of time-shift fluctuations using scattering theory of 2-D propagating waves in eq. (10) is then written as

$$\langle(\delta t)^2\rangle(L) = \int_{-\infty}^{\infty} \int_{-\infty}^{\infty} \int_0^L \int_0^L f(r)\eta(x', x'', z', z'')dx'dz'dx''dz''. \tag{C3}$$

The distance $r = \sqrt{l^2 + (z' - z'')^2}$ and $l = |x' - x''|$. We split the integration of the variable x'' in eq. (C3) into two parts; one integration from zero to x' and another integration from x' to L. The MS-value of time-shift fluctuations is then written as

$$\begin{aligned}\langle(\delta t)^2\rangle(L) = \int_{-\infty}^{\infty} dz' \int_{-\infty}^{\infty} dz'' \int_0^L dx' \\ \times \left[\int_0^{x'} f(r)\eta(x', x'', z', z'')dx'' \right. \\ \left. + \int_{x'}^{L} f(r)\eta(x', x'', z', z'')dx''\right]. \end{aligned} \tag{C4}$$

Define $l = x' - x''$ and $l = x'' - x'$ for the first and second integration of x'' inside the squared brackets, respectively. Making a change of variable, we obtain that

$$\begin{aligned}\langle(\delta t)^2\rangle(L) = \int_{-\infty}^{\infty} dz' \int_{-\infty}^{\infty} dz'' \int_0^L dx' \\ \times \left[\int_0^{x'} f(r)\eta(x', x' - l, z', z'')dl \right. \\ \left. + \int_0^{L-x'} f(r)\eta(x', x' + l, z', z'')dl\right]. \end{aligned} \tag{C5}$$

As shown explicitly in Appendix A of Spetzler & Snieder (2001a), we can change the order of integration of the variable x' and l in eq. (C5). Moreover, the auto-correlation function $f(r)$ depends on l and can be removed outside the squared brackets. The final result of the MS-value of time-shift fluctuations for waves propagating in 2-D media is written as

$$\begin{aligned}\langle(\delta t)^2\rangle(L) = \int_{-\infty}^{\infty} dz' \int_{-\infty}^{\infty} dz'' \int_0^L dl f\left(\sqrt{l^2 + (z' - z'')^2}\right) \\ \times \left[\int_l^L \eta(x', x' - l, z', z'')dx' \right. \\ \left. + \int_0^{L-l} \eta(x', x' + l, z', z'')dx'\right], \end{aligned} \tag{C6}$$

where we explicitly write $r = \sqrt{l^2 + (z' - z'')^2}$ in the auto-correlation function. Finally, we can investigate what happens to the scattering theoretical MS-value of time-shift fluctuations in the limit that the correlation length goes to zero. In that particular case, the auto-correlation function

$$f\left(\sqrt{l^2 + (z' - z'')^2}\right) = \begin{cases} (\varepsilon u_0)^2 & \text{if } z' = z'' \text{ and } l = 0 \\ 0 & \text{if } l \neq 0 \end{cases} \tag{C7}$$

We see that the auto-correlation function in eq. (C7) is only non-zero for the variable $l = 0$. This means that the MS-value of time-shift fluctuations using 2-D scattering theory converges towards zero in the limit that the correlation length goes to zero because the integration of the variable l in eq. (C6) yields zero.